*electronics*

MDPI

*Article*

# Control Strategy for Improving the Voltage Regulation Ability of Low-Carbon Energy Systems with High Proportion of Renewable Energy Integration

**Fei Liu [1,*], Yunfei Mu [1] and Zhe Chen [2]**

[1] School of Electrical and Information Engineering, Tianjin University, Tianjin 300072, China
[2] Department of Energy Technology, Aalborg University, DK-9000 Aalborg, Denmark
* Correspondence: three13304025262th@163.com

**Abstract:** In low-carbon energy systems, due to the high proportion of renewable energy access, the voltage regulation capacity of the system will decrease. Therefore, in the event of voltage violation, it is easy to cause large-scale renewable energy off-grid and power outages. In order to improve the voltage regulation ability of low-carbon energy system, this paper proposes a two-stage overvoltage suppression strategy for sending-end power grid. Firstly, the principle of overvoltage phenomenon in the sending end power grid of low-carbon energy system with high proportion of renewable energy access is studied, and an overvoltage control strategy composed of two stages of centralized control of rectifier station and flexible resource control of distributed power grid is proposed. Then, the PSO algorithm and consensus algorithm are used to solve the established control model. Finally, a simulation system is established based on actual operating power grid data to verify the proposed control strategy through simulation. The results indicate that the control strategy proposed in this paper can effectively suppress transient overvoltage of AC buses and improve the operational stability of the high proportion of renewable energy sending-end power grid under various operating conditions. In addition, during the daytime overvoltage regulation process, the potential of flexible regulation equipment can be fully utilized. Shortening the duration of voltage exceeding the limit and reducing the peak voltage exceeding the limit can help reduce the renewable energy waste rate of the power grid.

**Keywords:** high proportion of renewable energy; low-carbon energy systems; HVDC transmission; overvoltage control



**Citation:** Liu, F.; Mu, Y.; Chen, Z. Control Strategy for Improving the Voltage Regulation Ability of Low-Carbon Energy Systems with High Proportion of Renewable Energy Integration. *Electronics* **2023**, *12*, 2513. https://doi.org/10.3390/electronics12112513

Academic Editor: François Auger

Received: 19 April 2023
Revised: 20 May 2023
Accepted: 27 May 2023
Published: 2 June 2023



## 1. Introduction

Currently, low-carbon energy systems with large-scale renewable energy integration have shown significant economic and social benefits in pollution control, resource conservation, and environmental protection worldwide. However, the reverse distribution of renewable energy and load centers makes high-voltage direct current transmission an important way to consume renewable energy. Therefore, it is necessary to study the related issues faced by large-scale renewable energy access DC transmission systems.

When a large number of renewable energy sources are connected to the power grid of the DC transmission system, there are many risks in the actual operation of the power grid. On one hand, there is a strong coupling relationship between the DC and incoming AC systems, reducing the operational safety zone of the power grid. On the other hand, large-scale renewable energy integration has led to a decrease in the inertia of the DC near area power grid and an increase in the risk of cascading faults. This also increases the probability of black out in the grid where a high proportion of renewable energy is delivered. So, it is urgent to coordinate and optimize the power supply of the low-carbon energy system transmission end grid, and the establishment of a regulation system urgently needs improvement [1–3].

At present, the main measures taken to address the issue of the integration of renewable energy sources into the distribution network affecting voltage quality are still the traditional voltage regulation methods of the distribution network, including the use of on load voltage regulating transformers and the installation of reactive power compensation devices at specific points in the distribution network [4]. These schemes have not yet taken into account the regulating capacity of distributed power sources and energy storage devices in the system, and generally have problems such as limited regulating capacity, high operating and maintenance costs, and poor economic efficiency. Therefore, they are not suitable for power grids with a large number of distributed power sources [5].

At present, research on the suppression of system overvoltage mainly falls into two categories: equipment configuration optimization and control strategy optimization. In terms of voltage regulation equipment configuration research, reference [6] pre plans the reactive power absorption demand by configuring converter station condensers and filter capacitors to achieve the purpose of suppressing transient overvoltage.

Reference [7] proposes a method for implementing active power control in low-voltage power grids based on intelligent transformers. Reference [8] proposes an overvoltage suppression method for energy storage devices based on short-term response to shorten the overvoltage duration. The response duration of energy storage overvoltage suppression is controlled within a few milliseconds. Reference [9] proposes an adaptive droop control method for energy storage devices to stabilize the voltage of microgrid DC bus, with the energy storage SOC as the object of control. Reference [10] proposes a strategy for active and reactive power injection based on amplitude phase-locked loops. APLL-based spontaneous active and reactive power support can alleviate transient overvoltage and improve transient performance in the transmitting and receiving regions.

In terms of optimizing overvoltage suppression strategies, reference [11] proposes a reactive power controller based on sequential coordination method for voltage regulation in distribution systems. Reference [12] proposes a multi voltage level DC power grid partition voltage regulation method based on the power grid partition method, which significantly reduces the number of DC circuit breakers in the power grid. Reference [13] proposes a method to analyze the vulnerability of user equipment due to transient overvoltage using the transient voltage accumulation curve at the user end, ensuring the safe operation of users in the event of overvoltage.

Reference [14] proposes a constant reactive power control that increases the reactive power consumed by the rectifier, reduces the exchange of reactive power between AC and DC systems, and suppresses transient overvoltage. Reference [15] improves the global maximum power method identification method and proposes a maximum power point tracking method for photovoltaic systems, which improves the stability of the system. Reference [16] proposes a predictive coordinated voltage control method for high permeability photovoltaic (PV) unit distribution systems. Reference [17] proposes an integrated adaptive scheduling framework that coordinates distributed photovoltaic and energy storage systems to enhance system voltage regulation capabilities. Reference [18] proposes a new autonomous control framework called "Grid Mind", which uses DRL algorithm for training, enabling agents to formulate AVC strategies and take effective and timely control actions. Reference [19] proposes a deep learning intelligent system that combines power system STVSA data augmentation. Based on a small dataset, it achieves short-term voltage stability assessment of the power grid.

In summary, current research on the overvoltage of the power grid at the transmission end of low-carbon energy systems is mostly focused on individual equipment types [20], lacking research on collaborative operation control with the goal of fully utilizing the regulating potential of multiple equipment in the system, and unable to fully utilize the voltage regulating potential of low-carbon energy systems with large-scale renewable energy integration.

Therefore, from a global perspective, this article combines the system's flexible resource optimization control strategy with transient overvoltage and reactive power compensation

measures to jointly suppress overvoltage. This can fully utilize the automatic control and power tracking functions of photovoltaic inverters and multi energy storage devices in the system, leverage their advantages of sensitive response and fast action speed, and also reduce the additional investment cost of hardware equipment. To ensure the safe operation of the power grid for large-scale renewable energy integration, this paper proposes a two-stage overvoltage control strategy. Firstly, we analyze the overvoltage principle of the power grid at the transmitting end of high proportion renewable energy access, and clarify the transient overvoltage control objectives. To fully utilize the voltage regulation potential of the rectifier station condenser and the reactive power control potential of low-carbon energy systems, a two-stage overvoltage control model is established. Then, the control model is solved by combining the joint tuning method and consistency algorithm, and the voltage is adjusted by optimizing the parameters of the rectifier station condenser and adjusting the flexibility of the power grid to allocate reactive power back. Finally, the simulation results demonstrate the effectiveness of the control method proposed in this paper.

## 2. Two Stage Control of Grid Voltage at the Sending End of Low-Carbon Energy System

This article proposes a two-stage transient overvoltage control strategy for the sending-end power system of a low-carbon energy system with a high proportion of renewable energy integration. The coordinated control architecture is shown in Figure 1.

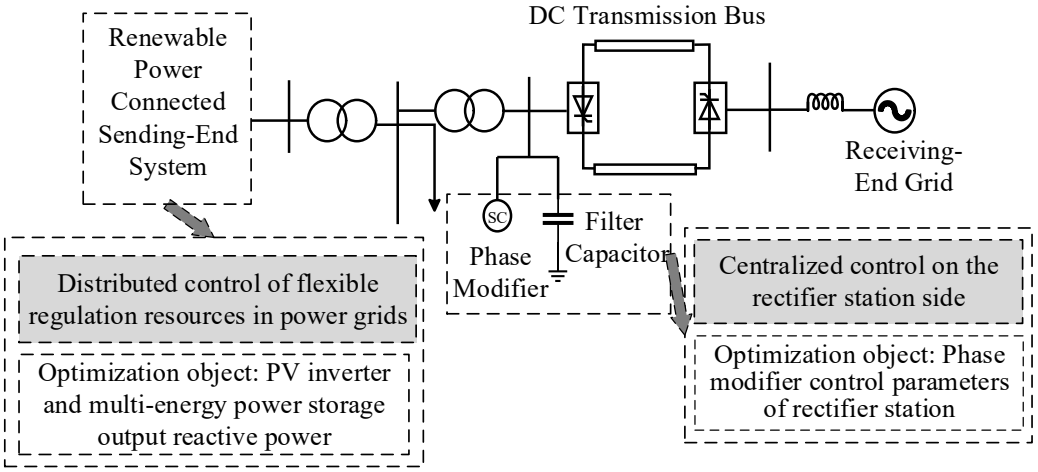


**Figure 1.** Two stage voltage control architecture.

The fundamental way to suppress overvoltage in the power grid at the sending end is to use voltage control equipment to absorb surplus reactive power in the power grid at the sending end. Therefore, when an overvoltage situation occurs, the two-stage control strategy proposed in this article optimizes the parameters of the rectifier station's condenser and flexibly adjusts the reactive power backoff allocation of resources through centralized control on the rectifier station side and flexible resource distributed control on the power grid, thereby completing the suppression of overvoltage.

(1) Centralized control on the rectifier station side. Due to the characteristics of the modifier itself, its internal reactive power response components can be divided into spontaneous reactive power components and excitation control reactive power components. The spontaneous reactive power component can be controlled without delay response, but the support of the excitation control component is required in the follow-up. There is a 20 ms delay when the excitation control reactive component starts. After the excitation control reactive power component is activated, the phase modifier enters the deep phase advance operation state. At this time, the reactive power adjustment capability of the phase modifier is fully activated.

(2) Flexible resource distribution control for power grid regulation. There are various types of flexible resource adjustment equipment in the low-carbon energy system's sending end grid [21,22]. This article mainly utilizes the advantages of fast response speed of photovoltaic inverters and various types of energy storage devices to coordinate photovoltaic inverters and multi-source energy storage to participate in the overvoltage control of the sending end system in the low-carbon energy system's sending end grid. On the basis of considering the control capacity of the phase modifier, the reactive power backoff burden is redistributed to further suppress the overvoltage of the power grid at the sending end.

### *2.1. Centralized Control Model on the Rectifier Station Side*

#### 2.1.1. Phase Modifier Control Model

On the rectifier station side, the control parameters of the modifiers are optimized, and then the voltage regulation and control of the excitation regulator of the modifier is performed. The transfer function of the excitation control system of the modifier can be expressed as:

$$G_{pm}(s) = \frac{(1+sT_1)(1+sT_3)}{(K_v+sT_2)(1+sT_4)(1+sT_e)(1+sT_a)} K_{pm}K_a \tag{1}$$

where $K_a$ is the phase modifier power amplifier gain; $K_{pm}$ is the phase modifier series correction link gain; $K_v$ is the phase modifier integral correction selection factor; $s$ is the phase modifier control component; $T_1, T_2, T_3, T_4, T_e, T_a$ are the time constant of serial correction link, measurement link, and power amplification link, respectively. The time constant of each link in the transfer function determines the delay time of the excitation response component.

The reactive power variation of the modifier $\Delta Q_{pm}$ can be considered as the sum of the spontaneous reactive power component $\Delta Q_{pm}^{au}$ and the excitation control reactive power component $\Delta Q_{pm}^{f}$. When the voltage of the AC bus of the sending end grid changes, the spontaneous reactive power component of the modifier automatically responds. Its reactive power instantaneous value calculation formula can be expressed as:

$$\Delta Q_{pm}^{au} = \Delta U_{t,0}^{ac} i_d - \frac{U_0^{ac} \cdot \Delta U_{t,0}^{ac}}{X_d'' + X_{pm}} \tag{2}$$

where $X_d'$ is the direct-axis subtransient reactance of the phase modifier; $\Delta U_{t,0}^{ac}$ is the difference between real-time voltage and steady-state voltage of AC bus of rectifier station; $U_0^{ac}$ is the steady-state voltage of AC bus of rectifier station; $X_{pm}$ is the phase modifier short-circuit reactance; $i_d$ is the phase modifier initial value of direct axis current.

After the overvoltage occurs, after a delay of 20 ms, the excitation control system of the camera starts to adjust, and the excitation reactive power control component can be expressed as:

$$\Delta Q_{pm}^{f} = \Delta U_{t,0}^{ac} i_d - U_0^{ac} \left[ T_f \cdot \Delta U_{t,0}^{ac} \right] \tag{3}$$

where $\Delta Q_{pm}^{f}$ is the phase modifier excitation reactive power control component; $T_f$ is the phase modifier excitation control system time parameter variable.

#### 2.1.2. Phase Modifier Parameter Optimization Method

(1) Phase modifier control objective function

In the control process of the phase modifier, the objective function is to take the lowest peak value of the AC bus voltage of the rectifier station as the objective function, and the controllable parameters in the phase modifier are adjusted in series with the correction link gain and the power amplification link gain as the adjustment object.

Since the scale of DC transmission power can directly affect the AC bus voltage of the rectifier station, it is necessary to consider the influence of different scales of DC transmission, and optimize the controllable parameters of the phase modifier. The objective function can be expressed as:

$$Z_1\left(P_d, K_a, K_{pm}\right) = \min\{U_{\max}^{ac}\} \tag{4}$$

where $P_d$ is DC transmission power; $U_{\max}^{ac}$ is AC bus transient overvoltage peak, it is taken as the particle fitness function $f_i(k)$ in the solution process.

(2) Restrictions

- *Phase modifier parameter constraint*

The upper and lower limits of the phase modifier parameters are constrained to be:

$$\begin{cases} K_{pm,\min} \le K_{pm} \le K_{pm,\max} \\ K_{a,\min} \le K_a \le K_{a,\max} \end{cases} \tag{5}$$

where $K_{pm,\min}$ and $K_{pm,\max}$ are the upper and lower limits of the gain of the phase modifier series correction link; $K_{a,\min}$ and $K_{a,\max}$ are the upper and lower limits of the power amplifier gain of the phase modifier.

- *Phase modifier capacity constraint*

When transient overvoltage occurs on the AC bus, the modifier should be in the under-excited state. The total amount of reactive power absorbed by it should be less than the maximum under-excitation capacity, so the capacity constraint of the phase modifier can be expressed as:

$$\frac{\left|Q_{pm,0} + \Delta Q_{pm}\right|}{m} = \frac{\left|Q_{pm,0} + \left(\Delta Q_{pm}^{au} + \Delta Q_{pm}\right)\right|}{m} \le Q_{pm,r} \tag{6}$$

where $Q_{pm,0}$ is the reactive power output by the phase modifier in steady state; $\Delta Q_{pm}$ is the difference between the output reactive power of the modifier before and after the transient overvoltage occurs; $Q_{pm,r}$ is the rated capacity of the phase modifier; $m$ is the multiple of the capacity compared to the rated state when the phase modifier works in the overexcitation state.

#### 2.1.3. Phase Modifier Parameter Optimization Solving Method

This article uses the PSO algorithm to optimize the parameters of the phase modifiers. Principle of the PSO algorithm is to abstract the elements in the optimization object into particles without mass and volume, and then form a population of these particles. In the population, the particles are screened by judging the fitness of the particles to the optimization target, and finally the optimal particle in the space is obtained, which is recorded as the optimal solution [23].

When the particles in the population are screened for the $(k+1)$th time, the updated velocity and position of each particle can be expressed as:

$$\begin{cases} \mathbf{v}_i(k+1) = w\mathbf{v}_i(k) + c_1 r_1(\mathbf{p}_b(k) - \mathbf{p}_i(k)) + c_2 r_2\left(\mathbf{p}_{\mathrm{g}}(k) - \mathbf{p}_i(k)\right) \\ \mathbf{p}_i(k+1) = \mathbf{p}_i(k) + \mathbf{v}_i(k) \end{cases} \tag{7}$$

where $\mathbf{v}_i(k+1)$ is the speed of particle $i$ update after the $(k+1)$th iteration; $\mathbf{p}_i(k)$, $\mathbf{v}_i(k)$ are the original position and velocity of particle $i$; $w$ is the inertia weights during iterative screening; $\mathbf{p}_b(k)$ is the original position of the individual optimal particle before this iteration; $c_1$, $c_2$ are learning factor at the $(k+1)$th iteration; $r_1$, $r_2$ are random constant; $\mathbf{p}_{\mathrm{g}}(k)$ are the original position of the global optimal particle before this iteration; $\mathbf{p}_i(k+1)$ is the updated position of particle $i$ after the $(k+1)$th iteration.

The improved PSO algorithm is used to optimize and update the control parameters of the phase modifier. The inertia weight calculation expression is as follows:

$$w_i(k) = \begin{cases} w_0 + (w_1 - w_0)\frac{f_i(k) - f_0}{f_a - f_0} & f_i(k) \leqslant f_a \\ w_1 & f_i(k) > f_a \end{cases} \tag{8}$$

where $w_i(k)$ is the inertia weight of particle $i$ at the kth iteration; $w_1$, $w_0$ are the maximum and minimum values that weights can take; $f_i(k)$ is the fitness function of particle $i$ at the kth iteration; $f_0$ is the lower limit of the fitness value of the particles; $f_a$ is the average fitness of the particles. When using the improved inertia weight function to iterate the particles, when the fitness value of particle $i$ is not less than the average value, select a small inertia weight to keep the particle near the global optimal point. Otherwise, choose the upper limit of the weight value to make the particle $i$ close to the global optimal point.

At present, most research on the control of rectifier station phase modifiers only focuses on optimizing control parameters, without considering the combination of the accuracy of time-domain simulation models and the efficiency of intelligent optimization algorithms. This cannot accurately reflect the dynamic characteristics of the control system while ensuring the efficiency of optimizing control parameters. Therefore, this article adopts the method of joint invocation to optimize and solve the parameters of the phase modifier [24].

The joint invocation method can combine the advantages of time-domain simulation and intelligent optimization algorithms. It updates the control parameters by calling the intelligent optimization algorithm (PSO algorithm in this article), and sends the updated control parameter values to the corresponding controller for time-domain simulation calculation. Therefore, it is possible to achieve data transfer and information exchange between each other, and the application principle is shown in Figure 2.

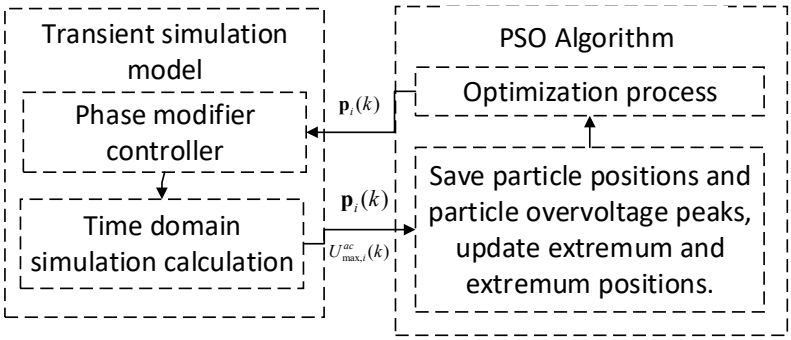


**Figure 2.** Joint invocation application principle.

The process of optimizing and solving phase modifier parameters based on joint invocation is divided into the following steps:

(1) Set the voltage data, simulation time for each particle, and control parameters to be optimized in the transient simulation model. Initialize particle swarm, set parameters for improved PSO algorithm, preset iteration accuracy, and upper and lower limits of control parameters to be optimized.

(2) Run a simulation program to sequentially insert the initial positions of particles into the electromagnetic transient model in time sequence for simulation. During operation, $U^{ac}_{\max}$ is calculated, and the individual optimal particle position $\mathbf{p}_b(k)$, individual optimal extreme value $p_b$, and the particle position corresponding to the particle with the smallest fitness function value of all particles $\mathbf{p}_s(k)$ are saved.

(3) Invoke improved PSO algorithm to update particle position, velocity, and inertia weights. Return the updated particle positions to the electromagnetic transient model for simulation.

(4) Determine whether the iteration accuracy meets the requirements. If it meets the requirements, the simulation ends and output $\mathbf{p}_s(k)$; If not, proceed to step (3).

### *2.2. Distributed Control Model for Power Grid Flexibility Regulation Resources*

At present, the droop control method is usually used to control the inverter output in the sending end grid inverter control. However, droop control will inevitably lead to DC bus voltage drop in the control process, and line impedance mismatch will affect the accuracy of current distribution.

For this reason, consensus algorithm is used to redistribute the reactive power back-off burden generated by PV inverters after AC bus transient overvoltage occurs, overcoming the defects of droop control. The principle of redistribution is to select the reactive power utilization rate of photovoltaic inverters as a consistency variable, and adjust the output reactive power of each photovoltaic inverter through information exchange between photovoltaic inverters [25].

The essence of the consensus algorithm is to update the state variables of local nodes through information interaction between local nodes and adjacent nodes, so that the state variables of nodes converge to stable common values. The controllable devices in the sending power grid interact with each other through the communication network to form a distributed communication network topology.

Communication topology can be described by directed graph:

$$G_c = \{V, \Upsilon\} \tag{9}$$

where $V$ represents the set of controllable devices, this paper represents photovoltaic inverters and multi-source energy storage devices. $\Upsilon \in V \times V$ represents the set of communication paths.

Let the state variable of node $m$ be $x_m(k)$, where $b$ is the number of iterations.$(m, n) \in V$ indicates that node $m$ can receive information from node $n$. In the control process, the state variables of each node are adjusted according to the state variables of its adjacent nodes. With the increase in the number of iterations, the state variables of the nodes tend to be consistent. When the state variables of all nodes reach consistency within the scope of convergence conditions, the system converges. The consensus algorithm can be described as:

$$x_m(b+1) = \sum_{n \in V} d_{mn} x_n(b) \tag{10}$$

where $d_{mn}$ is the state transition matrix coefficient; $V$ is the collection of nodes receiving information.

$$d_{mn} = \begin{cases} \frac{1}{1+D_m^a} & m = n \\ \frac{1}{1+D_m^a} & m \neq n, (m, n \in \Upsilon) \\ 0 & m \neq n, (m, n \notin \Upsilon) \end{cases} \tag{11}$$

where $D_m^a$ is the number of all nodes that can send information to node $m$.

#### 2.2.1. PV Inverter Model

The mathematical model of photovoltaic inverter can be expressed as:

$$\begin{cases} \dot{x} = f(x) + g_1(x)d + g_2(x)e \\ z = h(x) + k(x)e \end{cases} \tag{12}$$

where $x$ is the PV inverter state variables; $e$ is the PV inverter control variables; $d$ is the external disturbance, $g_1$, $g_2$ are the coefficient matrix for PV inverter disturbance and control variables; $z$ is the regulating PV inverter output; $h$, $k$ are the coefficient matrix for regulating PV inverter output, which adapted to target in practical application.

When the AC bus transient overvoltage occurs, the reactive power backoff burden of each PV inverter is distributed according to the consensus algorithm. In order to make

full use of the inverter capacity and distribute the voltage regulation tasks according to the inverter capacity, the reactive power utilization of the photovoltaic inverter is selected as the consistent variable. $u_{m,t}$ is the ratio of reactive output power and reactive capacity of PV inverter at node $m$, as:

$$u_{m,t} = \frac{Q_{\mathrm{PV},m,t}}{Q_{\mathrm{PV},m}^{\max}} \tag{13}$$

where: $Q_{\mathrm{PV},m,t}$ is the output power of photovoltaic inverter at node $m$ at time $t$;$Q_{\mathrm{PV},m}^{\max}$ is the maximum reactive output power of photovoltaic inverter at node $m$.

According to the consensus algorithm, the state variables of inverters in the network are updated according to the state variables of adjacent inverters. The reactive power utilization ratio $u_{m,t}(b)$ of the inverter at node $m$ at time $t$ is:

$$u_{m,t}(k) = \sum_{n \in V} d_{mn} u_{n,t}(b-1) \tag{14}$$

where $u_{n,t}(b-1)$ is the reactive power utilization result of the inverter at node $n$ adjacent to node $m$ after the last iteration.

According to the reactive power utilization results of photovoltaic inverters at each node obtained by iteration, it can be calculated that the reactive power required to be output by each photovoltaic inverter at time $t$ is:

$$Q_{\mathrm{PV},m,t}(b) = u_{m,t}(b) Q_{\mathrm{PV},m}^{\max} \tag{15}$$

2.2.2. Restrictions

- *PV inverter node voltage constraint*

$$V_{\min} \leqslant V_{m,t} \leqslant V_{\max} \tag{16}$$

where $V_{m,t}$ is the voltage of node $m$ at time $t$; $V_{\max}$ and $V_{\min}$ are the upper and lower limit of node voltage.

- *PV inverter reactive power control capacity constraint*

$$Q_{\mathrm{PV,min}} \leqslant Q_{\mathrm{PV}}(t) \leqslant Q_{\mathrm{PV,max}} \tag{17}$$

where $Q_{\mathrm{PV,max}}$ and $Q_{\mathrm{PV,min}}$ are the upper and lower limits of allowable output reactive power during inverter operation.

- *Power factor constraint of photovoltaic inverter grid connection point*

$$\cos \varphi_m \in [-1, -0.9] \cup [0.9, 1] \tag{18}$$

where $\varphi_m$ is the power factor angle of grid connected PV inverter at node $m$.

2.2.3. Distributed Control Model for Multi-Source Energy Storage

When centralized control on the rectifier station side is difficult to completely suppress overvoltage, multi-source energy storage devices in low-carbon energy systems will participate in overvoltage control [26]. This article focuses on the variation of SOC in multi-source storage $\Delta s$ as a consistency variable, S not only considers the difference in installed capacity of multi-source energy storage to ensure consistent changes in SOC of multi-source energy storage, but also achieves simultaneous control of multi-source energy storage power and SOC, reducing control complexity.

When the voltage of the dominant node exceeds the upper limit, the SOC increases while the energy storage is being charged; When the voltage of the dominant node exceeds

the lower limit, energy storage discharges while SOC decreases. The calculation of the energy storage SOC of the dominant node is shown as:

$$\Delta S_t^{\text{ref}}(k) = \begin{cases} \Delta S_t^{\text{ref}}(k-1) - c(V_{N,t}(k) - V_{\max}) & V_{N,t}(k) > V_{\max} \\ \Delta S_t^{\text{ref}}(k-1) & V_{\min} \leqslant V_{\text{N},t}(k) \leqslant V_{\max} \\ \Delta S_t^{\text{ref}}(k-1) - c(V_{N,t}(k) - V_{\min}) & V_{\text{N},t}(k) < V_{\max} \end{cases} \tag{19}$$

where $\Delta S_t^{\text{ref}}$ is the change in SOC of dominant node energy storage at time $t$; $c$ is the adjusting parameters for convergence speed and accuracy of control methods.

According to the iterative principle of the consistency algorithm, update $\Delta s$ of the energy storage device on node $m$ at time $t$:

$$\begin{aligned} \Delta S_{i,t}(b) &= \sum_{j \in \theta_{MES}} d_{ij} \Delta S_{j,t}(b-1) \\ &= \sum_{j \in \theta_{MES}, j \neq N} d_{ij} \Delta S_{j,t}(b-1) + d_{iN} \Delta S_t^{\text{ref}}(b-1) \end{aligned} \tag{20}$$

where $\theta_{MES}$ is the set of nodes connected to multi-source energy storage; $\Delta S_{j,t}$ is the variation of multi-energy storage SOC at time $t$ on node $j$.

Based on the change in SOC of multi-source energy storage, the active power of multi-source energy storage can be calculated as:

$$P_{MES,i,t}(b) = \frac{C_{MES,i} \Delta S_{i,t}(b)}{\Delta t} \quad i \in \theta_{MES} \tag{21}$$

where $P_{MES,i,t}$ is the active power of energy storage on node $i$ at time $t$; $C_{MES,i}$ is the energy storage capacity on node $i$; $\Delta t$ is the control time interval.

The SOC for multi-source energy storage at the next moment is:

$$S_{i,t+1} = S_{i,t} + \Delta S_{i,t} \quad i \in \theta_{MES} \tag{22}$$

2.2.4. Restrictions

- *Multi-energy storage SOC storage*

$$\underline{S} \leqslant S_{i,t} \leqslant \overline{S} \quad i \in \theta_{MES} \tag{23}$$

- *Multi-energy storage charging and discharging power constraints*

$$-P_{MES,i}^{\text{rated}} \leqslant P_{MES,i,t} \leqslant +P_{MES,i}^{\text{rated}} \quad i \in \theta_{MES} \tag{24}$$

where $P_{MES,i}^{\text{rated}}$ is the rated active power of energy storage device.

*2.3. Two-Stage Overvoltage Control Process*

In the centralized control model of the rectifier station side, this paper solves the parameter optimization process based on the joint invocation method. The solution process is shown in Section 2.1.3. The iterative calculation update $\mathbf{p}_i(k)$ is completed by PSO algorithm, and at the beginning of each simulation, it is imported into the controller corresponding to the transient simulation model for time domain simulation calculation. At the end of each simulation, the electromagnetic transient simulation model returns $\mathbf{p}_i(k)$ and $U_{\max}^{ac}$, then updates the extremum and extremum position.

In the distributed control model of flexible resources in the power grid, this paper solves the reactive power backoff of each photovoltaic inverter and the charging and discharging power of multi-source energy storage devices based on consistency algorithm. Firstly, measure the reactive power output and node voltage of each node inverter in the second iteration at time t, and then calculate the reactive power output required for each inverter and multi-source energy storage device based on the distributed control model

(Equations (11)–(23)). Control the reactive power output of each photovoltaic inverter and multi-source energy storage device, and the control is completed.

The overall solution process can be seen in Figure 3.

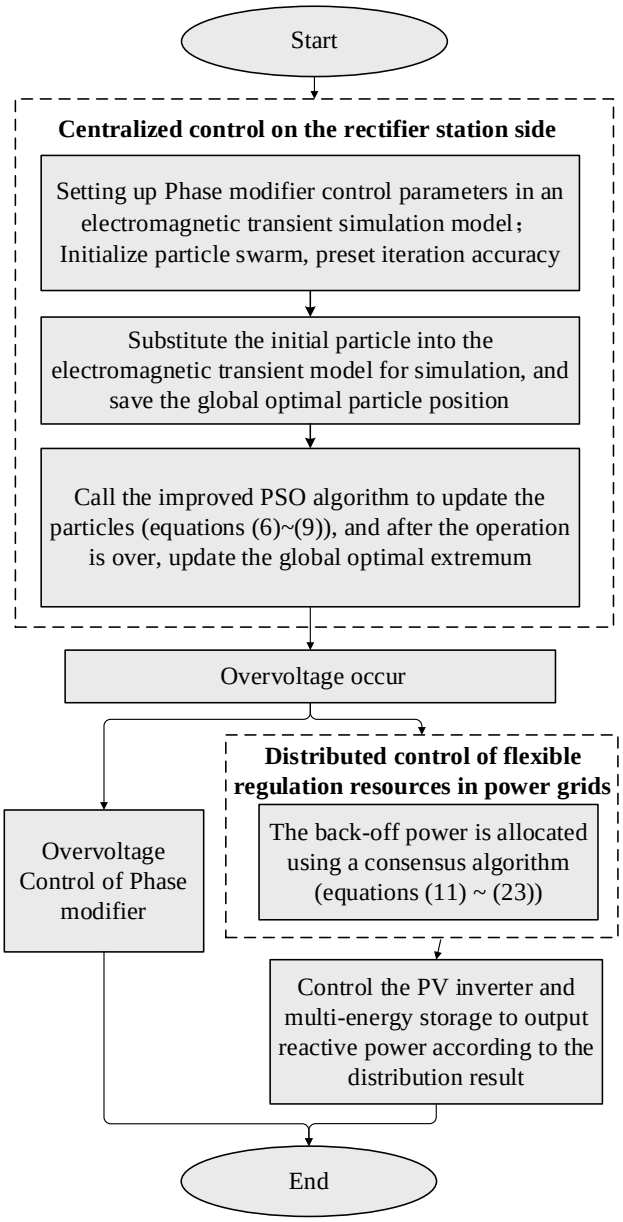


**Figure 3.** Two-stage overvoltage control process.

## 3. Simulation Analysis

For the scenario of high proportion renewable energy connected to DC transmission system, a simulation system for DC transmission of renewable energy connected to the transmission end is constructed as shown in Figure 4. Two supporting PV power stations and one wind power station are connected to the sending end system (4 × 100 MW, 4 × 102 MW, 3 × 103 MW). After step-by-step boosting, they are collected in three 750 kV substations. Among them, station2 is jointly built with the rectifier station, and the rectifier station is equipped with 8 phase modifiers which are 280 Mvar. The rated voltage of DC bus transmission is set to ±800 kV, and the rated power is set to 104 MW.

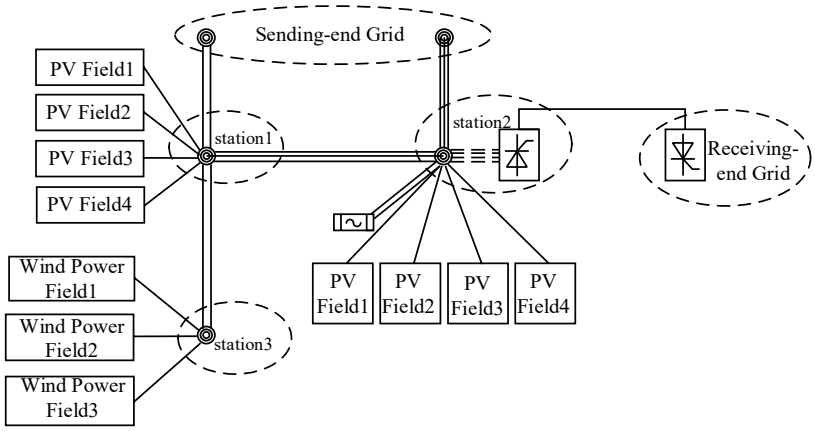


**Figure 4.** High-proportion renewable energy access to DC transmission system diagram.

To verify the effectiveness of the two-stage voltage control strategy proposed in this article, two simulation scenarios are set up: S1 is set as a transient overvoltage situation caused by a DC blocking fault in the power grid at the sending end; S2 is set as a typical daily voltage limit adjustment, where the voltage of the power grid at the sending end is adjusted during the typical day.

### *3.1. S1: Transient Overvoltage Caused by DC Blocking Fault*

It is set the transient over-voltage of AC bus caused by DC blocking fault to about 0.5s, and the voltage and current waveforms of the DC bus are shown in Figure 5.

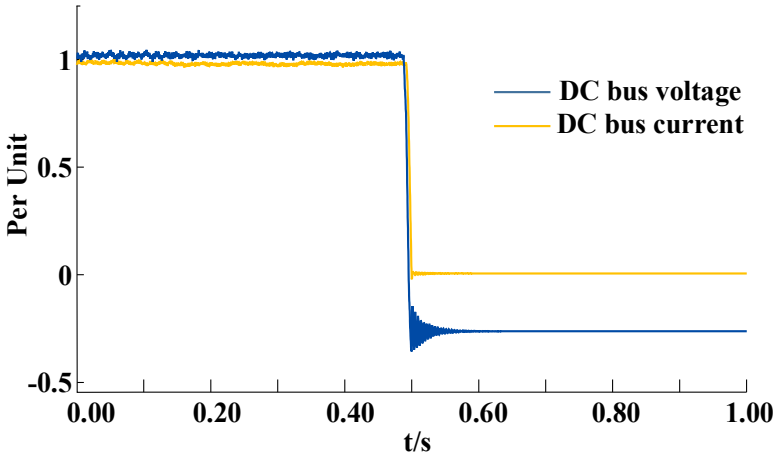


**Figure 5.** DC bus voltage and current waveforms.

It can be seen from Figure 5 that when the transient overvoltage condition occurs, the DC bus voltage and current sharply decrease to 0 p.u.

#### 3.1.1. S1.1: DC Low Power Transmission, Low Renewable Energy Output

Set the DC transmission power to 80 MW, connect wind power field 1, 2 and PV power station 2 to the power grid at the sending-end. Joint invocation method is used to solve the control model of the rectifier station side controller. The improved PSO algorithm needs to be called. Set the population size to 200, set the recombination probability to 0.6, set the operator crossover probability to 0.9, and set the number of iterations of the algorithm to 300. The values of the phase modifier control parameters before and after optimization are shown in Table 1.

**Table 1.** Phase modifier control parameter optimization results under S1.1.

| Parameter Status | Parameter | |
|---|---|---|
| | $K_{pm}$ | $K_a$ |
| Before optimization | 20.0 | 1.0 |
| After optimization | 38.0 | 2.6 |

It can be seen from Table 1 that after the parameters are optimized by using the parameter optimization method proposed in this paper, the gain of $K_{pm}$ and $K_a$ have been amplified to different degrees, respectively.

The results of the control model are output to the excitation regulator of the rectifier, and the change curves of the AC bus voltage on the rectifier station side and the reactive power output of the rectifier based on the control parameters before and after optimization are obtained, as shown in Figures 6 and 7.

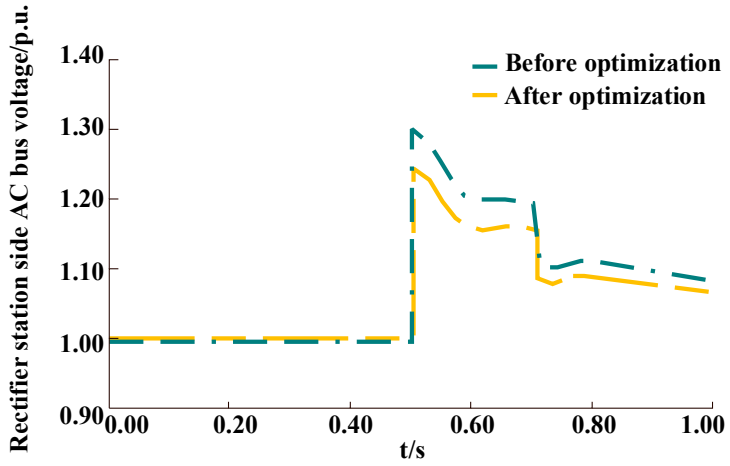


**Figure 6.** Rectifier station side AC bus voltage under S1.1.

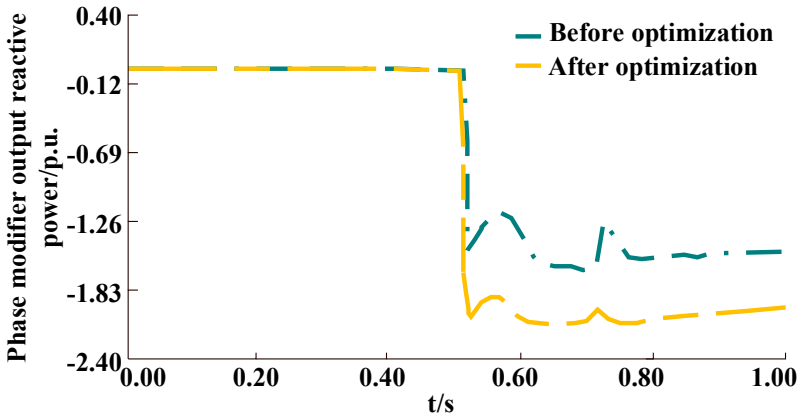


**Figure 7.** Phase modifier output reactive power under S1.1.

It can be seen from Figure 6 that after the parameters of the modifier are optimized using the parameter optimization strategy proposed in this paper, the peak voltage at the rectifier station side is reduced from 1.30 p.u. to 1.24 p.u. It alleviates the transient overvoltage problem of the sending-end power grid, and improves the reliability of the sending-end power grid operation. It can be seen from Figure 7 that after the parameter optimization control, the reactive power absorption potential of the condenser is fully released, and the response control performance during transient overvoltage is significantly improved. The effectiveness of the method proposed in this article under S1.1 is verified.

3.1.2. S1.2: DC High Power Transmission, Low Renewable Energy Output

Set the DC transmission power to rated power, connect wind power field 1, 2 and PV power station 2 to the power grid at the sending-end.

The values of the phase modifier control parameters before and after optimization are shown in Table 2.

**Table 2.** Phase modifier control parameter optimization results under S1.2.

| Parameter Status | Parameter | |
|---|---|---|
| | $K_{pm}$ | $K_a$ |
| Before optimization | 20.0 | 1.0 |
| After optimization | 44.0 | 5.5 |

From Table 2, it can be seen that compared to the optimization results of S1.1, the amplification degree of $K_{pm}$ and $K_a$ has slightly increased due to the increase in DC transmission power. The change curves of the AC bus voltage on the rectifier station side and the reactive power output of the rectifier based on the control parameters before and after optimization are obtained, as shown in Figures 8 and 9.

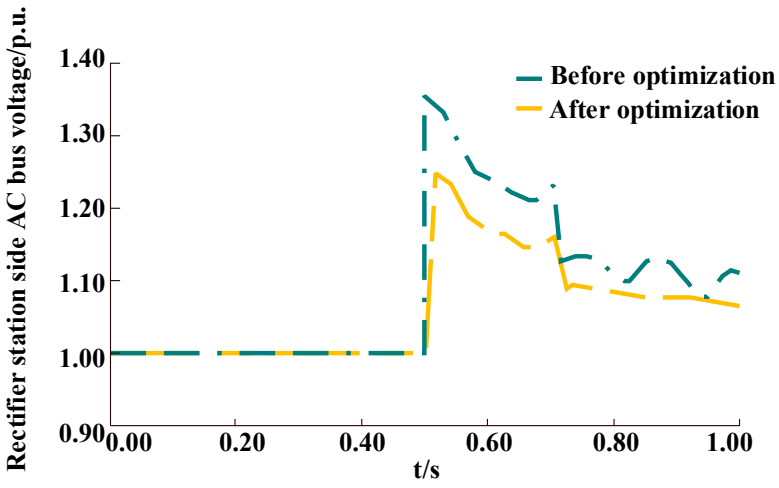


**Figure 8.** Rectifier station side AC bus voltage under S1.2.

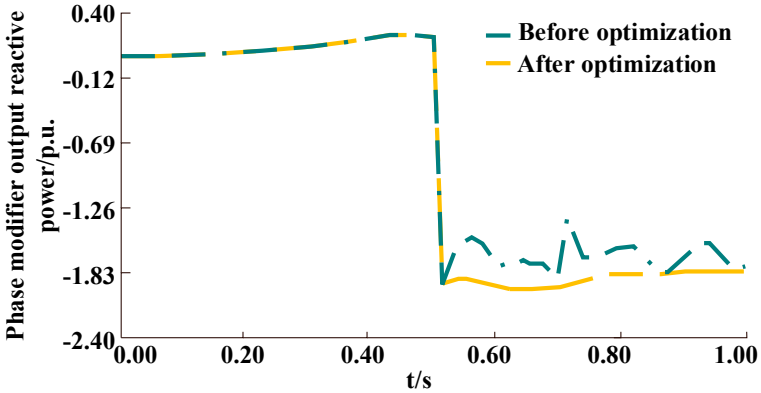


**Figure 9.** Phase modifier output reactive power under S1.2.

From Figures 8 and 9, it can be seen that when the DC output power is high, the peak voltage on the rectifier station side before optimization is 1.35 p.u., which is higher than S1.1. After using the parameter optimization strategy proposed in this article to optimize the parameters, the peak voltage was reduced to 1.24 p.u., which is basically consistent

with the optimized voltage peak in S1.1, which verifies that the parameter optimization method proposed in this article is still effective when the DC output power is high, and can ensure the reliable operation of the power grid at the sending end.

#### 3.1.3. S1.3: DC High Power Transmission, High Renewable Energy Output

Set the DC transmission power to rated power, connect wind power field 1, 2, 3 and PV power station 1, 2 to the power grid at the sending-end.

The values of the phase modifier control parameters before and after optimization are shown in Table 3.

**Table 3.** Phase modifier control parameter optimization results under S1.3.

| Parameter Status | Parameter | |
|---|---|---|
| | $K_{pm}$ | $K_a$ |
| Before optimization | 20.0 | 1.0 |
| After optimization | 49.7 | 8.4 |

From Table 3, it can be seen that in order to cope with the demand for high DC output and high renewable energy output, the optimized results of $K_{pm}$ and $K_a$ have the highest values under three operating conditions. The change curves of the AC bus voltage on the rectifier station side and the reactive power output of the rectifier based on the control parameters before and after optimization are obtained, as shown in Figures 10 and 11.

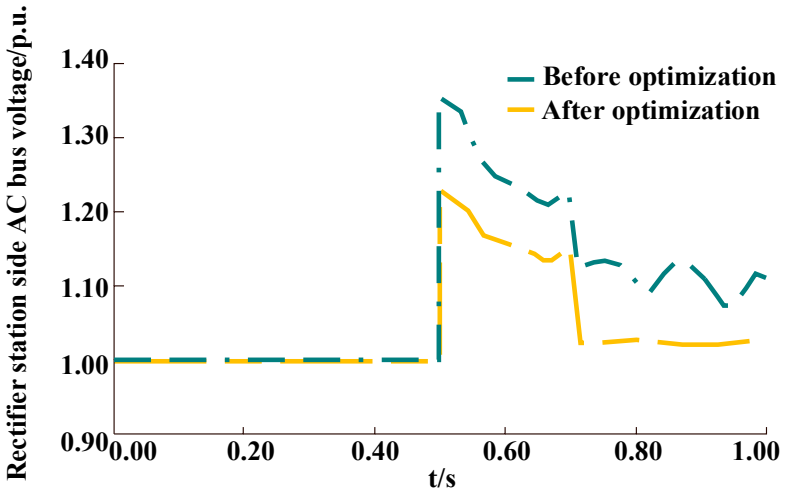


**Figure 10.** Rectifier station side AC bus voltage under S1.3.

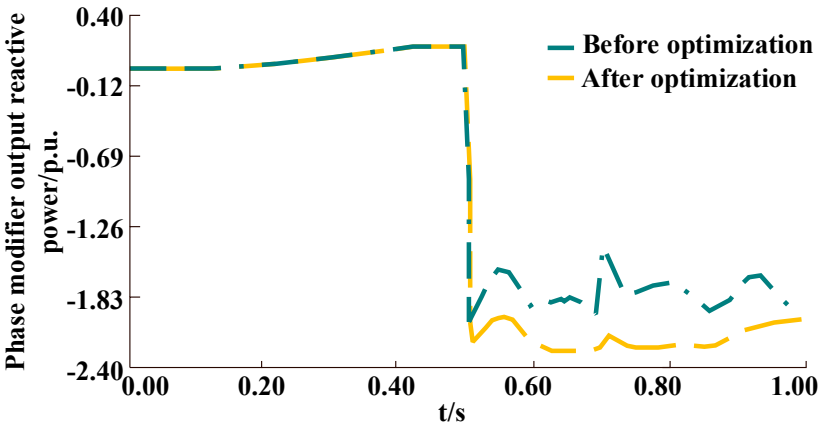


**Figure 11.** Phase modifier output reactive power under S1.3.

From Figures 10 and 11, it can be seen that after parameter optimization control, the response control performance of the phase modifier during transient overvoltage is significantly improved. Similar to S1.1 and S1.2, the optimized phase modifier can significantly alleviate the transient overvoltage problem of the power grid at the sending end, and improve the reliability of the power grid operation at the sending end.

Therefore, the voltage control method proposed in this article can achieve voltage control without delay after the occurrence of transient overvoltage. Furthermore, it enhances the operational stability of the high proportion of renewable energy transmission to the power grid, prevents large-scale renewable energy disconnection caused by transient overvoltage, and reduces the probability of black out.

### *3.2. S2: Typical Daily Voltage Exceeding Limit Regulation of the Power Grid at the Sending End*

Figure 12 shows the variation of the average voltage of the power grid nodes at the sending end during a typical day. From Figure 12, it can be seen that there are two voltage limit exceeding periods in the sending-end power grid during typical days, namely 8:40 to 13:40 and 17:00 to 22:20 time periods.

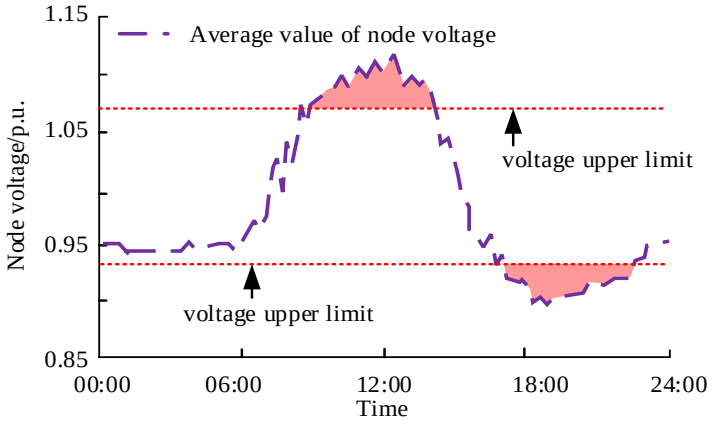


**Figure 12.** Typical daily node voltage curve of the low-carbon energy system's sending-end power grid.

To verify the superiority of the voltage control method proposed in this article, the scenario where the control strategy proposed in this article is used for voltage control is denoted as S2.1; Compare the photovoltaic inverter and energy storage coordination local control strategy proposed in Reference [27], denoted as S2.2.

The output curve of the photovoltaic inverter and the state of charge curve of the multi-source energy storage device during the adjustment process are shown in Figures 13–15.

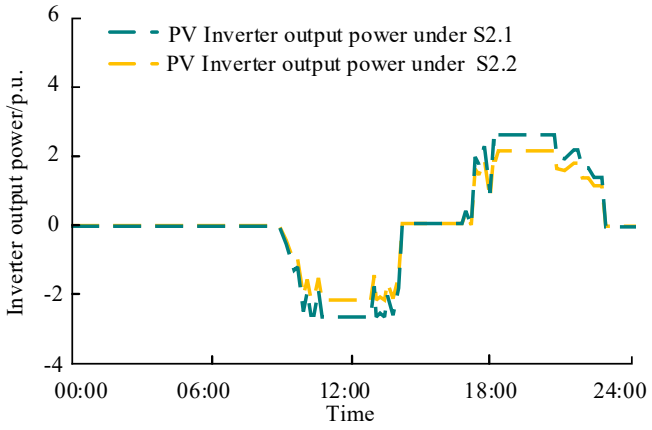


**Figure 13.** Inverter output curve.

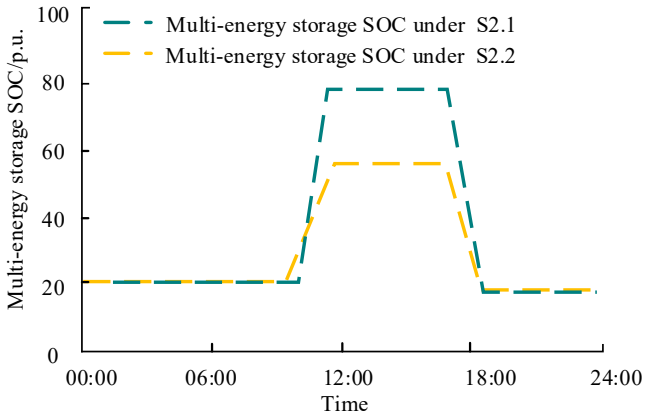


**Figure 14.** Multi-energy storage SOC curve.

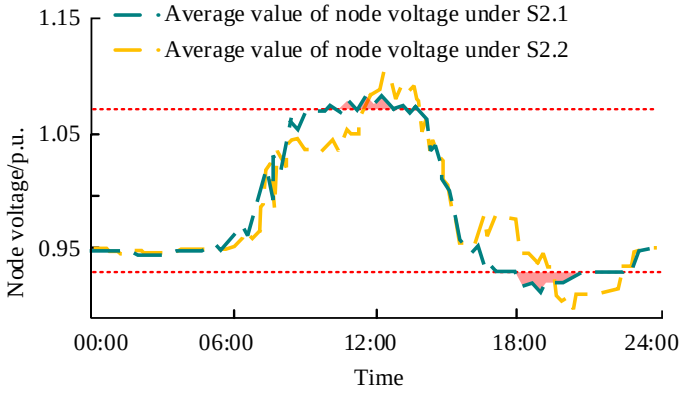


**Figure 15.** Node voltage curve under two-stages control strategy.

From Figure 13, it can be seen that when using the voltage control strategy proposed in this article to regulate the voltage of the power grid at the sending end, the photovoltaic inverter participates in voltage regulation during both voltage limit exceeding periods. Compared to the local control strategy, the consensus control strategy proposed in this article can better unleash the voltage regulation potential of photovoltaic inverters. From Figure 14, it can be seen that under the two control strategies, the charging and discharging depths of the energy storage device are different. Under the local control strategy, different nodes adopt a unified control curve, which leads to a lack of coordination in energy storage output. Some energy storage nodes' voltage changes far below the upper and lower voltage limits, resulting in waste of energy storage regulation capacity.

From Figure 15, it can be seen that under both control strategies, the overvoltage duration of the power grid at the sending end is significantly shortened, and the overvoltage peak value is reduced. However, obviously, under the control strategy from this article, the suppression effect of overvoltage is more obvious. Voltage peak decreases from 1.12 to 1.09 during the upper limit stage, and the valley value increases from 0.90 to 0.92 during the lower limit stage. The superiority of the voltage control strategy proposed in this article in typical daily voltage limit exceeding regulation is verified.

## 4. Conclusions and Prospect

This paper proposes a two-stage voltage control strategy for the voltage regulation of the low-carbon energy system with a high proportion of renewable energy integration. A simulation system was constructed to verify the effectiveness of the proposed voltage regulation method, and the following conclusion is drawn:

(1) In the case of transient overvoltage, the two-stage voltage control method proposed in this article can suppress the AC bus voltage of the power grid without delay

by optimizing the parameters of the phase modifier. Furthermore, it enhances the operational stability of the high proportion of renewable energy transmission to the power grid, prevents large-scale renewable energy disconnection caused by transient overvoltage, and reduces the probability of black out.

(2) The two-stage voltage control strategy proposed in this article can fully leverage the potential of flexible regulation equipment in the sending end power grid when the typical daily voltage exceeds the limit. It could shorten the duration of voltage exceeding the limit and reduce the peak value of voltage exceeding the limit. Therefore, it helps to extend the service life of power grid equipment, reduce the waste rate of renewable energy from the transmission end of the power grid, and effectively improve the economic efficiency of low-carbon power system operation.

However, from the simulation results in the article, it can be seen that after using the control strategy proposed in this article, there are still a few moments when the voltage exceeds the limit. This is because the reactive power capacity and energy storage depth of the photovoltaic inverter have reached the limit at these times, so the voltage exceeding the limit cannot be completely eliminated. Therefore, further research is needed on how to more thoroughly suppress overvoltage situations. At present, machine learning algorithms are widely used in the planning and management of energy systems around the world. However, in future research, it is also feasible to study the voltage suppression of sending-end power grids with high proportion of new energy access based on machine learning algorithms.

**Author Contributions:** This article was written by F.L., who carried out the design and data analysis of the main research, Y.M. led the writing of the article, and Z.C. gave guidance to the paper. All authors have made contributions to the writing and revision of the article, and have suggestions for improvement to ensure that the article can accurately express complex research results. All authors have read and agreed to the published version of the manuscript.

**Funding:** This research received no external funding.

**Data Availability Statement:** The simulation analysis part of this article is based on real operating power grid data, and for confidentiality reasons, the data in this article will not be disclosed.

**Conflicts of Interest:** The authors declare no conflict of interest.

## References

1. Qin, B.Y.; Li, H.Y.; Zhang, Z. Underground space supported electric energy systems: Conceptions, challenges, and prospects. *Proc. CSEE* **2022**, *42*, 1321–1332.
2. Liu, Z.; Zhang, Q.; Dong, C.; Zhang, L.; Wang, Z. Efficient and security transmission of wind, photovoltaic and thermal power of large-scale energy resource bases through UHVDC projects. *Proc. CSEE* **2014**, *34*, 2513–2522.
3. Li, Y.; Gao, D.W.; Gao, W.; Zhang, H.; Zhou, J. Double-Mode Energy Management for Multi-Energy System via Distributed Dynamic Event-Triggered Newton-Raphson Algorithm. *IEEE Trans. Smart Grid* **2020**, *11*, 5339–5356. [CrossRef]
4. Ren, C.; Ke, X.; Fan, G.; Liu, X.; Lu, H. Transient voltage attabilization and control optimization for large-scale wind power UHVDC transmission system. *High Volt. Electr. Equip.* **2020**, *56*, 163–174.
5. Wang, N.; Sun, L.; Jia, Q.; Cui, Z. Chance constrained programming method of distributed photovoltaic grid connection considering PV voltage regulation ability. *Adv. Technol. Electr. Eng. Energy* **2018**, *37*, 88–96.
6. Zhao, R.; Ke, D.; Sun, Y.; Xu, J.; Chang, H.; Liu, F. Efficient reactive power planning of converter station in HVDC sending system considering HVDC blocking transient overvoltage constraint. *S. Power Syst. Technol.* **2022**, 1–12.
7. Giacomuzzi, S.; Langwasser, M.; De Carne, G.; Buja, G.; Liserre, M. Smart transformer-based medium voltage grid support by means of active power control. *CES Trans. Electr. Mach. Syst.* **2020**, *4*, 285–294. [CrossRef]
8. Hu, A.; Zhuang, J.; Tao, Y.; Yang, J.; Zhou, C. A Voltage Sag Suppression Method with Short Response Time Based on Energy Storage System. In Proceedings of the 2019 IEEE 3rd International Electrical and Energy Conference (CIEEC), Beijing, China, 7–9 September 2019; pp. 1854–1859. [CrossRef]
9. He, X.; Ji, H.; Song, Y.; Song, G.; Cai, H.; Mi, Y. Voltage stability control for DC microgrid with energy storage. In Proceedings of the 2017 IEEE Conference on Energy Internet and Energy System Integration (EI2), Beijing, China, 26–28 November 2017; pp. 1–6. [CrossRef]
10. Shang, L.; Hua, Z.; Liu, C.; Dong, X. Amplitude-Phase-Locked-Loop-Based Power Injection Strategy for Wind Power Generation Under Three-Phase Grid Fault. *IEEE Trans. Energy Convers.* **2022**, *37*, 2952–2961. [CrossRef]

11. Aboshady, F.; Ceylan, O.; Zobaa, A.F.; Ozdemir, A.; Taylor, G.; Pisica, I. Sequentially Coordinated and Cooperative Volt/Var Control of PV Inverters in Distribution Networks. *Electronics* **2023**, *12*, 1765. [CrossRef]
12. Han, Y.; Ma, R.; Li, T.; Zeng, W.; Liu, Y.; Wang, Y.; Guo, C.; Liao, J. Fault Detection and Zonal Protection Strategy of Multi-Voltage Level DC Grid Based on Fault Traveling Wave Characteristic Extraction. *Electronics* **2023**, *12*, 1764. [CrossRef]
13. Homaee, O.; Sobbouhi, A.; Gholami, A.; Vahedi, A. A Conservative Approach for Investigation of Transient Overvoltage Acceptability in Customers' Terminals by Considering Voltage Vulnerability Curves of Customers. *IEEE Trans. Energy Convers.* **2018**, *33*, 1590–1593. [CrossRef]
14. Yin, C.; Li, F. Reactive Power Control Strategy for Inhibiting Transient Overvoltage Caused by Commutation Failure. *IEEE Trans. Power Syst.* **2021**, *36*, 4764–4777. [CrossRef]
15. Ahmad, W.; Qureshi, M.B.; Khan, M.M.; Fayyaz, M.A.B.; Nawaz, R. Optimizing Large-Scale PV Systems with Machine Learning: A Neuro-Fuzzy MPPT Control for PSCs with Uncertainties. *Electronics* **2023**, *12*, 1720. [CrossRef]
16. Mahdavi, S.; Panamtash, H.; Dimitrovski, A.; Zhou, Q. Predictive Coordinated and Cooperative Voltage Control for Systems with High Penetration of PV. *IEEE Trans. Ind. Appl.* **2021**, *57*, 2212–2222. [CrossRef]
17. Shi, D.; Sharma, R.K. Adaptive control of energy storage for voltage regulation in distribution system. In Proceedings of the 2013 IEEE International Conference on Smart Energy Grid Engineering (SEGE), Oshawa, ON, Canada, 13–15 August 2013; pp. 1–7. [CrossRef]
18. Duan, J.; Shi, D.; Diao, R.; Li, H.; Wang, Z.; Zhang, B.; Bian, D.; Yi, Z. Deep-Reinforcement-Learning-Based Autonomous Voltage Control for Power Grid Operations. *IEEE Trans. Power Syst.* **2020**, *35*, 814–817. [CrossRef]
19. Li, Y.; Zhang, M.; Chen, C. A Deep-Learning intelligent system incorporating data augmentation for Short-Term voltage stability assessment of power systems. *Appl. Energy* **2022**, *308*, 118347. [CrossRef]
20. Li, B.; Chao, P.; Xu, S. Review on transient overvoltage issues of wind power transmission system via UHVDC. *Electr. Power Autom. Equip.* **2022**, *42*, 26–35.
21. Li, Y.; Zhang, H.; Liang, X.; Huang, B. Event-triggered based distributed cooperative energy management for multi-energy systems. *IEEE Trans Ind. Inf.* **2019**, *15*, 2008–2022. [CrossRef]
22. Li, Y.; Gao, D.W.; Gao, W.; Zhang, H.; Zhou, J. A Distributed Double-Newton Descent Algorithm for Cooperative Energy Management of Multiple Energy Bodies in Energy Internet. *IEEE Trans. Ind. Inform.* **2021**, *17*, 5993–6003. [CrossRef]
23. Gong, Y.J.; Li, J.J.; Zhou, Y.; Li, Y.; Chung, H.S.H.; Shi, Y.H.; Zhang, J. Genetic Learning Particle Swarm Optimization. *IEEE Trans. Cybern.* **2015**, *46*, 2277–2290. [CrossRef]
24. Zhinong, W.E.I.; Xinmin, M.I.A.O.; Huawei, W.A.N.G. Parameter Optimization for HVDC Control System Based on PSCAD-MATLAB Combined Invocation. *High Volt. Eng.* **2014**, *40*, 2449–2455. [CrossRef]
25. Olfati-Saber, R.; Fax, J.A.; Murray, R.M. Consensus and Cooperation in Networked Multi-Agent Systems. *Proc. IEEE* **2007**, *95*, 215–233. [CrossRef]
26. Teng, Y.; Sun, P.; Hui, Q.; Li, Y.; Chen, Z. A model of electro-thermal hybrid energy storage system for autonomous control capability enhancement of multi-energy microgrid. *CSEE J. Power Energy Syst.* **2019**, *5*, 489–497. [CrossRef]
27. Wei, T.; Yongxiang, C.; Tianrui, L.; Ouyang, X.U. Distributed PV consumption control strategy and performance analysis in low voltage distribution network. *Distrib. Energy* **2018**, *3*, 1–12.